A unified mathematical model for low-cost integrated navigation systems

R. González [a†], J.I. Giribet [b] and , H.D. Patiño [c]

[a]*Electronics Department, National Technological University. Rodriguez 273, M5502AJE, Mendoza, Argentina*;
[b]*Electronics Department, University of Buenos Aires. Av. Paseo Colón 850, C1063ACV, Buenos Aires, Argentina*;
[c]*Institute of Automation, National University of San Juan, Av. San Martin Oeste 1112, J5400ARL, San Juan, Argentina*

Abstract

New solutions to the navigation problem related to low-cost integrated navigation systems are often proposed in the literature. Since these new solutions are compared with different mathematical models, one can not be sure of the relative improvements. In this work, a unified mathematical model (UMM) for low-cost integrated navigation systems is presented. As far as we know, there is a lack of an UMM for low-cost integrated navigation systems. Our UMM comprises a strapdown inertial navigation system with magnetometers, loosely-coupled to a GPS receiver. Since our UMM is intended to be used as a benchmark, it is based on both classical navigation equations and classical sensor models. To validate our UMM, we take real-world data sets from three MEMS inertial measurement units and a GPS receiver, and process them using our UMM. We find that obtained RMS errors for the three integrated systems are coherent with the quality of corresponding sensors, which confirms the validity of our UMM.

Index Terms

navigation; system modelling; inertial sensors; signal and information processing; aerospace systems; robotic systems

I. Introduction

An integrated navigation system is an electronic device mainly composed of an onboard computer, an inertial measurement unit (IMU), which contains accelerometers and gyroscopes, in addition to aiding sensors such as a GPS receiver and magnetometers. It provides estimates of position and velocity, as well as orientation parameters for a moving platform. Recently, with advances in Micro Electro-Mechanical Systems (MEMS) technology, low-cost, commercial-off-the-shelf, MEMS-based inertial sensors are available. Integrated navigation systems based on MEMS inertial sensors are a subject of great interest today due to their unique characteristics, such as light weight, low power consumption, and low cost, which make them suitable for several applications, e.g., positioning of flying and land robots.

New solution approaches to the navigation problem related to low-cost integrated navigation systems are often proposed in the literature. For instance, modifications to nonlinear filters to estimate system states or novel integration strategies. Since new solutions from different authors are usually compared with different mathematical models, one can not be sure of the relative improvements. Moreover, these new solutions are contrasted with ad-hoc mathematical models which are not fully shown, commonly by space restrictions, and thus it is very difficult to replicate the exposed results (e.g. see [1], [2]). In some cases, navigation data are processed using proprietary software which usually does not reveal mathematical models (e.g. see [3]). A unified mathematical model (UMM) could be a useful tool to constrast new solutions for low-cost integrated navigation systems against a particular reference model, and to obtain fair numerical comparisons. The use of an UMM as a benchmark would lead to obtain unbiased conclusions about the advantage of new navigation solutions for low-cost integrated navigation systems.

In this paper, a unified mathematical model for low-cost integrated navigation systems is presented. It consists of a strapdown inertial navigation system (SINS) with magnetometers (SINS/MAG system), loosely-coupled to a GPS receiver (SINS/MAG/GPS system), and an extended Kalman filter (EKF) to accomplish the fusion of inertial sensors, magnetometers, and GPS. The algorithm that explains the sequence in which equations must be solve is also provided.

To the best of our knowlegde, there is a lack of a unified mathematical model for low-cost integrated navigation systems. The main contribution of our work is to proposed an UMM for low-cost integrated navigation systmens. We believe that this is the first work that proposed an UMM for low-cost integrated navigation systems.

A loosely-coupled SINS/GPS system is chosen between other types of integration schemes since it can be implemented with most low-cost GPS receivers. Besides, our UMM is mechanized into the navigation frame (n-frame) because position in this frame is represented in a more intuitive way, and, in addition, this frame has the property that horizontal and vertical errors are decoupled.

[†]Corresponding author. Email: rodralez@frm.utn.edu.ar

Due to recognized authors of integrated navigation literature expose mathematical models with some differences, our UMM takes the best approaches from each one. As said, our UMM is intended to be used as a benchmark, thus it is based on both classical navigation equations and classical sensor models. Besides, our UMM is in the discrete-time domain to be easily programmed in any programming language to comparison purpose.

We validate our UMM taking a practical approach. Field data was collected using MEMS inertial measurement units (IMU) and a GPS receiver. We set up three integrated navigation systems using data sets from three different MEMS IMU and the GPS. Reference values are obtained fusing a navigation-grade IMU and DGPS measurements. Then, we process the three integrated navigation systems using our UMM and analyze the resulting systems performances.

The rest of this paper is organized as follows. Section II shows mathematical models of sensors. Section III exhibits the mathematical model of a loosely-coupled integrated navigation system, including EKF equations. Section IV shows the UMM algorithm. In Section V, method to validate our UMM is explained. Finally, in Section VI concluding remarks are commented.

II. Sensors mathematical models

This sectios exposes the mathematical models of inertial and aiding sensors.

All the equations presented in this and coming sections are in the discrete-time domain, except clarification. Besides, being the current interval sample t_k, variables with subscript $(-)$ correspond to the former interval sample, $t_{(k-1)}$. Otherwise, variables with subscript $(+)$ belong to the later interval sample, $t_{(k+1)}$. Noisy measurements have as superscript a tilde ($\sim$). Estimated variables calculated based on noisy measurements have as superscript a hat ($\wedge$).

A skew symmetric matrix operator is defined as $S_{\{3\times3\}} = [\boldsymbol{r}\times]$ where $\boldsymbol{r}_{\{3\times1\}}$ is a vector [4, Eq. B.15, p. 463].

A. Gyroscopes

Outputs of orthogonal triaxial gyroscopes are modelled as,

$$\tilde{\boldsymbol{\omega}}^b = \boldsymbol{\omega}_{ib}^b + \boldsymbol{\eta}_g + \boldsymbol{b}_g + \boldsymbol{\eta}_{g\delta b}\,. \tag{1}$$

where $\boldsymbol{\omega}_{ib}^b$ represents the ideal gyroscopes outputs [5, Eq. 3.29, p. 32], and the rest of terms represent different types of errors.

A gyroscope has several source of errors as random noise, rate random walk, rate ramp, bias, cross-coupling errors, scale factor, and axes misalignments, among others. Our UMM takes only three errors into account which we consider dominant over others: noise, static and dynamic biases [6, Sec. 4.4.1, p. 113]. Noise of gyroscopes can be expressed as Gaussian white noise sequences $\boldsymbol{\eta}_g \sim \mathrm{N}(\boldsymbol{0}, \boldsymbol{\sigma}_g^2)$, where $\boldsymbol{\sigma}_g^2 = [\sigma_{gx}^2, \sigma_{gy}^2, \sigma_{gz}^2]^T$. Usually, gyroscopes manufacturers deliver random noise as angle random walk parameter (ARW) in units of root PSD. If ARW is $\boldsymbol{N}\left(\frac{\text{deg}}{\sqrt{\text{h}}}\right)$, then [4, Sec. 4.6.3.2, p. 135],

$$\boldsymbol{n}_g = \frac{\boldsymbol{N}}{60}\frac{\pi}{180}\left(\frac{\text{rad/s}}{\sqrt{\text{Hz}}}\right)\,. \tag{2}$$

Static bias $\boldsymbol{b}_g$ varies every time the gyroscope is turned on, but stays constant throughout operation, hence it is modelled as a random constant. On the other hand, dynamic bias $\delta\boldsymbol{b}_g$ is usually observed at low frequencies and is associated with a correlation time $\boldsymbol{\tau}_g$ and variance $\boldsymbol{\sigma}_{g\delta b}^2$. Thus, it is modeled as a Gauss-Markov process.

B. Accelerometers

The proposed error model of accelerometers is similar to the error model of gyroscopes, presented in Eq. 1,

$$\tilde{\boldsymbol{f}}^b = \boldsymbol{f}^b + \boldsymbol{\eta}_f + \boldsymbol{b}_f + \boldsymbol{\eta}_{f\delta b} \tag{3}$$

where $\boldsymbol{\eta}_f \sim \mathrm{N}(\boldsymbol{0}, \boldsymbol{\sigma}_f^2)$ with variance $\boldsymbol{\sigma}_f^2 = [\sigma_{fx}^2, \sigma_{fy}^2, \sigma_{fz}^2]^T$. $\boldsymbol{b}_f$ denotes the static bias and $\boldsymbol{\eta}_{f\delta b}$ indicates the dynamic bias noise modeled as a Gauss-Markov process with correlation time $\boldsymbol{\tau}_f$ and variance $\boldsymbol{\sigma}_{f\delta b}^2$.

Generally, accelerometers random noise is given as velocity random walk (VRW). Thus, if VRW is $\boldsymbol{N}\left(\frac{\text{m/s}}{\sqrt{\text{h}}}\right)$, then,

$$\boldsymbol{n}_f = \frac{\boldsymbol{N}}{60}\left(\frac{\text{m/s}^2}{\sqrt{\text{Hz}}}\right)\,. \tag{4}$$

C. Magnetometers

Orthogonal triaxial magnetometers are modelled as,

$$\tilde{\boldsymbol{m}}^b = \boldsymbol{m}^b + \boldsymbol{\eta}_m \,. \tag{5}$$

Vector $\boldsymbol{m}^b$, ideal magnetometers measurements, are added with Gaussian white noise sequences $\boldsymbol{\eta}_m \sim \mathrm{N}(\mathbf{0}, \boldsymbol{\sigma}_m^2)$, whose variance is $\boldsymbol{\sigma}_m^2 = [\sigma_{mx}^2, \sigma_{my}^2, \sigma_{mz}^2]^T$.

Precision specification of magnetometers are also commonly given in units of root PSD as $\boldsymbol{n}_m \left(\frac{\mathrm{mG}}{\sqrt{\mathrm{Hz}}}\right)$.

D. GPS receiver

1) GPS position: A low-cost GPS receiver usually delivers estimates of position in the navigation frame (n-frame) as $\tilde{\boldsymbol{p}}_{GPS}^n = [\tilde{\gamma}_{GPS}, \tilde{\lambda}_{GPS}, \tilde{h}_{GPS}]^T$ where $\tilde{\gamma}_{GPS}$ denotes geodetic latitude, $\tilde{\lambda}_{GPS}$ denotes geodetic longitude, both in radians, and $\tilde{h}_{GPS}$ denotes geodetic altitude in meters above the reference ellipsoid [4, Sec. 2.3.2.1, p. 29].

A GPS receiver delivers estimates of position with certain dispersion. GPS position is considered to be added with Gaussian white noises sequences $\eta_\gamma \sim \mathrm{N}(0, \sigma_\gamma^2)$, $\eta_\lambda \sim \mathrm{N}(0, \sigma_\lambda^2)$, and $\eta_h \sim \mathrm{N}(0, \sigma_h^2)$, as,

$$\tilde{\gamma}_{GPS} = \gamma + \eta_\gamma \tag{6a}$$

$$\tilde{\lambda}_{GPS} = \lambda + \eta_\lambda \tag{6b}$$

$$\tilde{h}_{GPS} = h + \eta_h \,. \tag{6c}$$

Usually, GPS manufacturers give horizontal position accuracy expressed as circular error probable (CEP) in meters, which is the radius of the circle centered on the correct location that contains 50% of the expected horizontal position errors [4, Sec. 4.9.1.2, p. 149]. Considering that latitude σ_γ and longitude σ_λ standard deviations are equals, then [4, Table 4.2, p. 154],

$$\sigma_\gamma = \sigma_\lambda = 0.8493 \cdot \mathrm{CEP\ (m)} \,. \tag{7}$$

2) GPS velocity: Additionally, most low-cost GPS receivers provide estimates of velocity in the vehicle-carried NED frame [7, Sec. 2.2.4, p. 27].

GPS velocity vector $\tilde{\boldsymbol{v}}_{GPS}^n = [\tilde{v}_{N_{GPS}}, \tilde{v}_{E_{GPS}}, \tilde{v}_{D_{GPS}}]^T$ is modelled as true NED velocity $\boldsymbol{v}^n = [v_N, v_E, v_D]^T$ plus Gaussian white noise sequences $\boldsymbol{\eta}_v \sim \mathrm{N}(\mathbf{0}, \boldsymbol{\sigma}_v^2)$, where $\boldsymbol{\sigma}_v^2$ is given by the GPS manufacturer, as,

$$\tilde{\boldsymbol{v}}_{GPS} = \boldsymbol{v}^n + \boldsymbol{\eta}_v \,. \tag{8}$$

III. Integrated navigation mathematical model

This section presents the mathematical model of a loosely-couple strapdown inertial navigation system, in addition to an extended Kalman filter (EKF) equations to fusion navigation information.

A. Strapdown inertial navigation system

A strapdown inertial navigation system (SINS) is an electronic device rigidly mounted on a vehicle, compound of a computer and inertial sensors (accelerometers and gyroscopes) whose axis are aligned respect to the vehicle body frame (b-frame), to continuously calculate estimates of orientation, position, and velocity. Fig. 1 shows a diagram of a SINS with magnetometers.

1) Turn rates: Table I shows some important constants from the World Geodetic System 1984 (WGS84) Earth model to be used next.

Table I
Constants from WGS84 Earth model.

Name	Symbol	Value	
Semi-major axis	a	6378137.0	m
Semi-minor axis	b	6356752.3142	m
Eccentricity	e	0.0818191908426	
Earth angular rate	Ω	7.292115E-5	rad/s

The turn rate of the Earth expressed in the navigation frame is [5, Eq. 3.72, p. 47],

$$\hat{\boldsymbol{\omega}}_{ie}^n = \left[\Omega \cos \hat{\gamma}_{(-)}, 0, -\Omega \sin \hat{\gamma}_{(-)}\right]^T \,. \tag{9}$$

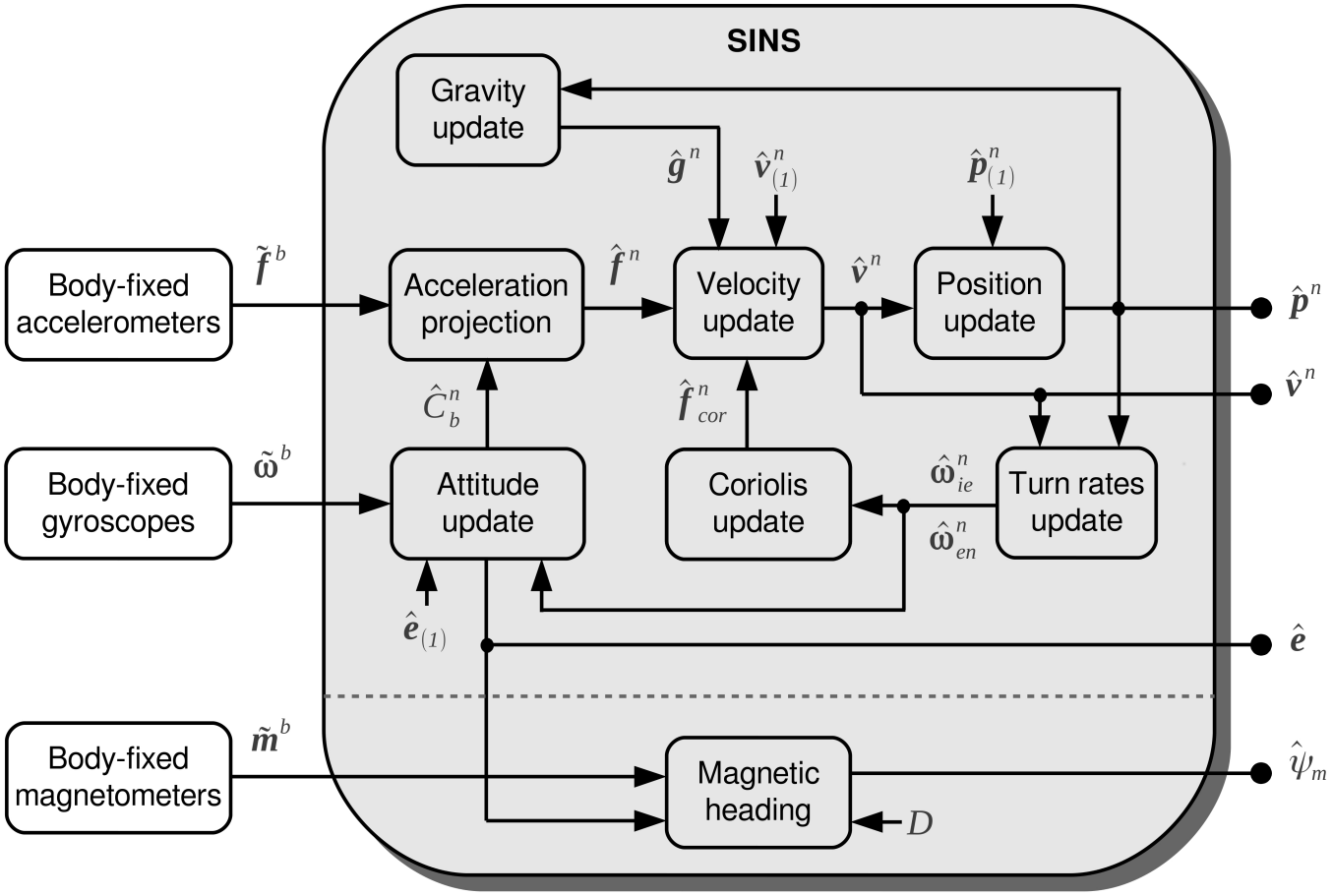

Figure 1. Diagram of a strapdown inertial navigation system with magnetometers.

The turn rate of the n-frame respect to the Earth expressed in the n-frame, known as the transport rate, is [5, Eq. 3.74, p. 47],

$$\hat{\boldsymbol{\omega}}^n_{en} = \left[\frac{\hat{v}_{E(-)}}{\hat{R}_{N(-)} + \hat{h}_{(-)}}, \frac{-\hat{v}_{N(-)}}{\hat{R}_{M(-)} + \hat{h}_{(-)}}, \frac{-\hat{v}_{E(-)} \tan \hat{\gamma}_{(-)}}{\hat{R}_{N(-)} + \hat{h}_{(-)}} \right]^T \tag{10}$$

where R_M is the meridian radius of curvature [5, Eq. 3.83, p. 49] and R_N is the normal radius of curvature [5, Eq. 3.84, p. 49], expressed as,

$$\hat{R}_M = \frac{a\,(1-e^2)}{(1-e^2 \sin^2 \hat{\gamma})^{3/2}} \tag{11a}$$

$$\hat{R}_N = \frac{a}{(1-e^2 \sin^2 \hat{\gamma})^{1/2}}\,. \tag{11b}$$

2) Attitude: Quaternion attitude representation is selected to propagate changes in body orientation. This method presents better precision and avoids singularities when compared with other methods such as direction cosine matrix. A quaternion vector is represented by,

$$\boldsymbol{q} = [\ \boldsymbol{\varrho},\ q_4\ ]^T = [q_1,\ q_2,\ q_3,\ q_4]^T \tag{12}$$

where q_1, q_2, q_3, and q_4 are real numbers. A quaternion has a vector part, $\boldsymbol{\varrho} = [q_1,\ q_2,\ q_3]^T$, and a scalar part, q_4, and satisfies the constraint given by $\boldsymbol{q}^T\boldsymbol{q} = 1$. Initial quaternion $\hat{\boldsymbol{q}}_{(1)}$ can be obtained from estimation of Euler angles, typically at rest (see [5, Eq. 3.65, p. 46]).

Equations to update quaternions $\hat{\boldsymbol{q}}$ from gyroscopes measurements are [8, Eq. 7.39, p. 458],

$$\hat{\boldsymbol{\omega}}_c^b = \tilde{\boldsymbol{\omega}}^b - \hat{C}_{n(-)}^b(\hat{\boldsymbol{\omega}}_{ie}^n + \hat{\boldsymbol{\omega}}_{en}^n) + \hat{\boldsymbol{b}}_{g(-)} + \delta\hat{\boldsymbol{b}}_{g(-)} \tag{13a}$$

$$= [\hat{\omega}_{cx}^b,\, \hat{\omega}_{cy}^b,\, \hat{\omega}_{cz}^b]$$

$$m = \|\hat{\boldsymbol{\omega}}_c^b\| \tag{13b}$$

$$c_1 = \frac{\hat{\omega}_{cx}^b}{m}\,\sin(0.5\,m\,\delta t) \tag{13c}$$

$$c_2 = \frac{\hat{\omega}_{cy}^b}{m}\,\sin(0.5\,m\,\delta t) \tag{13d}$$

$$c_3 = \frac{\hat{\omega}_{cz}^b}{m}\,\sin(0.5\,m\,\delta t) \tag{13e}$$

$$c_4 = \cos(0.5\,m\,\delta t) \tag{13f}$$

$$\hat{\boldsymbol{q}} = \begin{bmatrix} c_4 & c_3 & -c_2 & c_1 \\ -c_3 & c_4 & c_1 & c_2 \\ c_2 & -c_1 & c_4 & c_3 \\ -c_1 & -c_2 & -c_3 & c_4 \end{bmatrix} \hat{\boldsymbol{q}}_{(-)} \tag{13g}$$

$$\hat{\boldsymbol{q}} = \frac{\hat{\boldsymbol{q}}}{\|\hat{\boldsymbol{q}}\|}\,. \tag{13h}$$

Vector $\tilde{\boldsymbol{\omega}}^b$ are the outputs of three orthogonal gyroscopes (Eq. 1). The time between measurements is δt. Vectors $\hat{\boldsymbol{b}}_g$ and $\delta\hat{\boldsymbol{b}}_g$ are provided by the EKF (Eq. 20f). The updated quaternion $\hat{\boldsymbol{q}}$ is a unit vector to within first-order. Commonly, a brute-force normalization should be performed to insure $\boldsymbol{q}^T\boldsymbol{q} = 1$ (Eq. 13h).

A direction cosine matrix $\hat{C}_{b\{3\times3\}}^n$ is needed for projecting measurements from the b-frame to the n-frame. Elements of $\hat{C}_b^n$ are updated using quaternions as follows [5, Eq. 3.63, p. 45],

$$\hat{C}_{b(1,1)}^n = \hat{q}_1^2 - \hat{q}_2^2 - \hat{q}_3^2 + \hat{q}_4^2 \tag{14a}$$

$$\hat{C}_{b(1,2)}^n = 2(\hat{q}_1\hat{q}_2 - \hat{q}_3\hat{q}_4) \tag{14b}$$

$$\hat{C}_{b(1,3)}^n = 2(\hat{q}_1\hat{q}_3 + \hat{q}_2\hat{q}_4) \tag{14c}$$

$$\hat{C}_{b(2,1)}^n = 2(\hat{q}_1\hat{q}_2 + \hat{q}_3\hat{q}_4) \tag{14d}$$

$$\hat{C}_{b(2,2)}^n = -\hat{q}_1^2 + \hat{q}_2^2 - \hat{q}_3^2 + \hat{q}_4^2 \tag{14e}$$

$$\hat{C}_{b(2,3)}^n = 2(\hat{q}_2\hat{q}_3 - \hat{q}_1\hat{q}_4) \tag{14f}$$

$$\hat{C}_{b(3,1)}^n = 2(\hat{q}_1\hat{q}_3 - \hat{q}_2\hat{q}_4) \tag{14g}$$

$$\hat{C}_{b(3,2)}^n = 2(\hat{q}_2\hat{q}_3 + \hat{q}_1\hat{q}_4) \tag{14h}$$

$$\hat{C}_{b(3,3)}^n = -\hat{q}_1^2 - \hat{q}_2^2 + \hat{q}_3^2 + \hat{q}_4^2\,. \tag{14i}$$

Roll ($\hat{\phi}$), pitch ($\hat{\theta}$), and yaw ($\hat{\psi}$) angles are updated using matrix $\hat{C}_b^n$, respectively, as [5, Eq. 3.66, p. 46],

$$\hat{\phi} = \arctan\left[\hat{C}_{b(3,2)}^n / \hat{C}_{b(3,3)}^n\right] \tag{15a}$$

$$\hat{\theta} = \arcsin\left[-\hat{C}_{b(3,1)}^n\right] \tag{15b}$$

$$\hat{\psi} = \arctan2\left[\hat{C}_{b(2,1)}^n, \hat{C}_{b(1,1)}^n\right]\,. \tag{15c}$$

3) Gravity: Equations to evaluate the estimated local gravity into the n-frame are [5, Eq. 3.89–3.91, p. 57],

$$\hat{R}_0 = \sqrt{\hat{R}_M\,\hat{R}_N} \tag{16a}$$

$$\hat{g}(0) = g_0\left(1 + g_1\sin^2\left(\hat{\gamma}_{(-)}\right) - g_2\sin^2\left(2\,\hat{\gamma}_{(-)}\right)\right) \tag{16b}$$

$$\hat{g} = \frac{\hat{g}(0)}{\left(1 + \dfrac{\hat{h}_{(-)}}{\hat{R}_{0(-)}}\right)^2} \tag{16c}$$

$$\hat{\boldsymbol{g}}^n = [0,\ 0,\ \hat{g}]^T\,. \tag{16d}$$

Table II shows the constants used in Eq. 16b.

4) Velocity: SINS velocity $\hat{\boldsymbol{v}}^n = [\hat{v}_N, \hat{v}_E, \hat{v}_D]^T$, in units of meters per second, is represented in the vehicle-carried North-East-Down (NED) coordinate system [7, Sec. 2.2.4, p. 27]. $\hat{\boldsymbol{v}}^n$ is determined by the following equations [5, Eq. 3.69, p. 47],

Table II
CONSTANTS FOR GRAVITY ESTIMATION.

g_0	9.780318
g_1	5.3024E-3
g_2	5.9E-6

$$S = [\hat{\boldsymbol{v}}^n_{(-)} \times] \tag{17a}$$
$$\hat{\boldsymbol{f}}^n_c = \hat{C}^n_b \left(\tilde{\boldsymbol{f}}^b + \hat{\boldsymbol{b}}_{f(-)} + \delta\hat{\boldsymbol{b}}_{f(-)} \right) \tag{17b}$$
$$\Delta\boldsymbol{f}^n = \hat{\boldsymbol{f}}^n_c + S\left(2\,\hat{\boldsymbol{\omega}}^n_{ie} + \hat{\boldsymbol{\omega}}^n_{en}\right) + \hat{\boldsymbol{g}}^n \tag{17c}$$
$$\hat{\boldsymbol{v}}^n = \hat{\boldsymbol{v}}^n_{(-)} + \Delta\boldsymbol{f}^n \delta t \tag{17d}$$

where vector $\tilde{\boldsymbol{f}}^b$ contains the outputs of three orthogonal accelerometers (Eq. 3), and vectors $\hat{\boldsymbol{b}}_f$ and $\delta\hat{\boldsymbol{b}}_f$ are given by the EKF (Eq. 20f).

5) Position: As with GPS sensor, SINS position is represented in the navigation frame (n-frame) as $\hat{\boldsymbol{p}}^n = [\hat{\gamma}, \hat{\lambda}, \hat{h}]^T$. Estimation of $\hat{\boldsymbol{p}}^n$ is calculated in a specific order as [5, Eq. 3.79–3.81, p. 48],

$$\hat{h} = \hat{h}_{(-)} - \hat{v}_D \;\delta t \tag{18a}$$
$$\hat{\gamma} = \hat{\gamma}_{(-)} + \frac{\hat{v}_N \;\delta t}{\hat{R}_{M(-)} + \hat{h}} \tag{18b}$$
$$\hat{\lambda} = \hat{\lambda}_{(-)} + \frac{\hat{v}_E \;\delta t}{\left(\hat{R}_N(\hat{\gamma}) + \hat{h}\right)\cos\hat{\gamma}}\,. \tag{18c}$$

6) Magnetic heading angle: The magnetic heading angle is calculated based on magnetometers measurements and represents the number of radians between the nose of the vehicle and the magnetic north, not the real north. Consequently, this value is corrected using the local declination D, which represents the difference in radians between the real north and the magnetic north. The corrected magnetic heading angle is used to initialize $\hat{\psi}$ and to correct it of on a regular basis.

The magnetic heading angle is calculated as follows. Components of the Earth magnetic field in the horizontal plane are represented as [9, Eq. 2],

$$\begin{bmatrix} \hat{m}^h_x \\ \hat{m}^h_y \end{bmatrix} = \begin{bmatrix} \cos\hat{\theta} & \sin\hat{\phi}\sin\hat{\theta} & -\cos\hat{\phi}\sin\hat{\theta} \\ 0 & \cos\hat{\phi} & \sin\hat{\phi} \end{bmatrix} \begin{bmatrix} \tilde{m}_x \\ \tilde{m}_y \\ \tilde{m}_z \end{bmatrix} \tag{19a}$$

where $\tilde{\boldsymbol{m}}^b = [\tilde{m}_x, \tilde{m}_y, \tilde{m}_z]^T$ are orthogonal magnetometers measurements.

Thus, the corrected magnetic heading angle is,

$$\hat{\psi}_m = \arctan2\left(\hat{m}^h_y, \hat{m}^h_x\right) + D\,. \tag{19b}$$

Since D changes over position and time, it can be taken as constant only for certain trajectories.

The magnetic heading accuracy $\sigma_{\psi m}$ is another important value given by magnetometers manufacturers, which states the expected differences in degrees between true heading and $\hat{\psi}_m$.

B. Extended Kalman filter

The Kalman filter is an algorithm for linear systems that operates recursively on noisy input and output data to produce a statistically optimal estimate of the system states. The extended Kalman filter (EKF) is a nonlinear extension of the Kalman filter, which linearizes about an estimate of the current mean and covariance.

In our UMM, the states of the EKF are error-oriented. Hence, the algorithm fuses information coming from inertial and aiding sensors to get state estimates with less errors when compared with using sensors separately. The SINS error model is obtained by perturbing the mechanization equations (Sec. III-A), and is given by a series of first order differential equations. The resulting system is linear although time-variant. Fig. 2 exposes how the SINS/MAG/GPS system and the EKF work together. It can be seen from Fig. 2 that corrections in $\hat{\boldsymbol{x}}$ are fed back and used it as prior information to calculate estimates at the SINS (feedback integration).

The continuous state-space model of the system in time domain is [10, Sec. 7.1, p. 290],

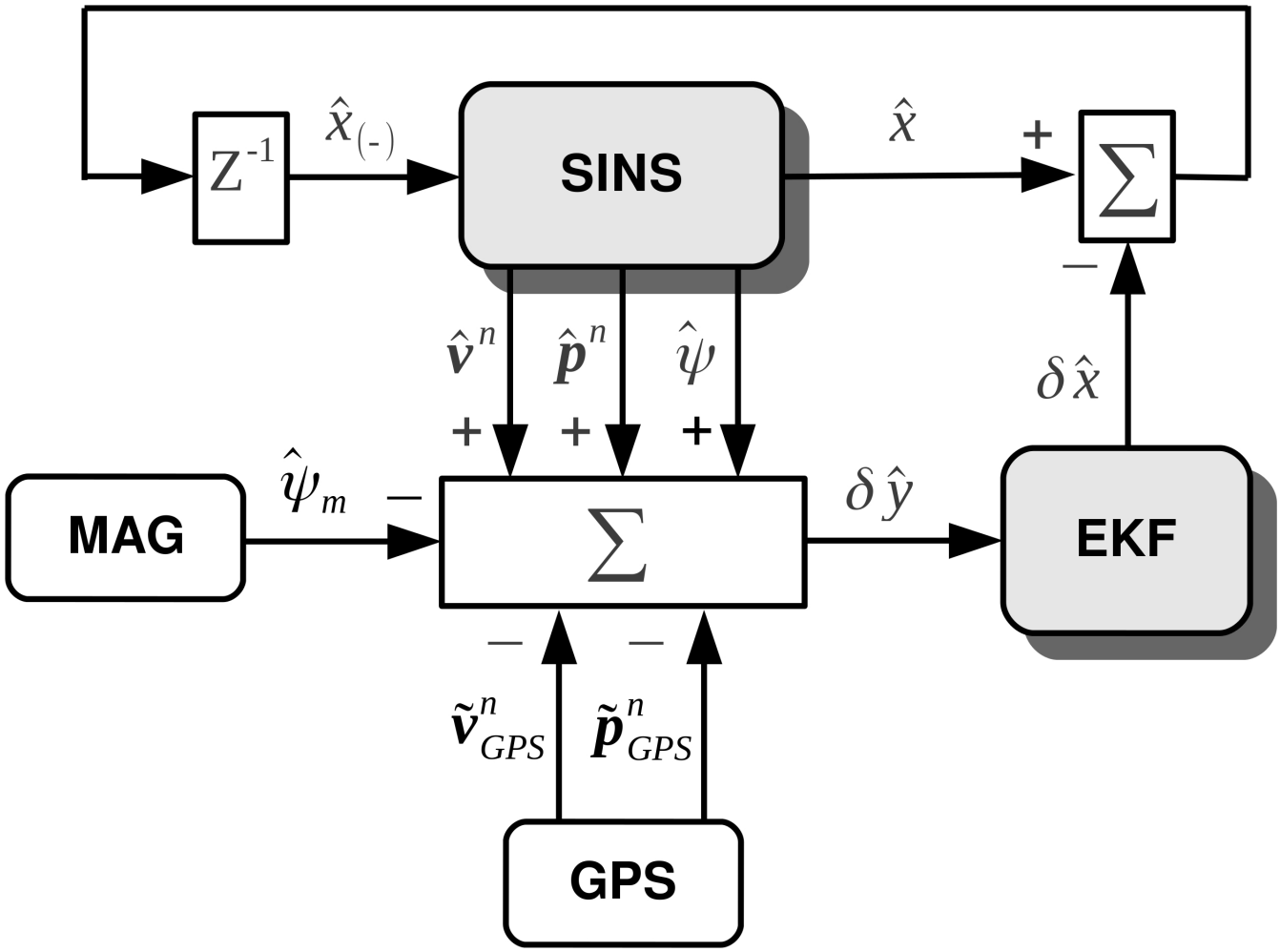

Figure 2. Diagram of EKF and SINS/MAG/GPS system integration.

$$\delta\dot{\hat{\boldsymbol{x}}}_{(t)} = F_{(t)}\,\delta\hat{\boldsymbol{x}}_{(t)} + G_{(t)}\,\boldsymbol{u}_{(t)} + \boldsymbol{\zeta}_{(t)} \tag{20a}$$

$$\delta\hat{\boldsymbol{y}}_{(t)} = H\,\delta\hat{\boldsymbol{x}}_{(t)} + \boldsymbol{\nu}_{(t)}\,. \tag{20b}$$

The discrete state-space model of the system is [10, Sec. 5.5, p. 214],

$$\delta\hat{\boldsymbol{x}}_{(+)} = \Phi\,\delta\hat{\boldsymbol{x}} + G\,\boldsymbol{u} + \boldsymbol{\zeta} \tag{20c}$$

$$\delta\hat{\boldsymbol{y}} = H\,\delta\hat{\boldsymbol{x}} + \boldsymbol{\nu}\,. \tag{20d}$$

Vectors $\boldsymbol{\zeta} \sim \mathrm{N}(\mathbf{0}, Q)$ and $\boldsymbol{\nu} \sim \mathrm{N}(\mathbf{0}, R)$, Gaussian distributions with zero mean and known covariance matrix, are known as driving noise and measurement noise, respectively. Vectors $\boldsymbol{u} \in \mathbb{R}^{12}$, $\delta\hat{\boldsymbol{x}} \in \mathbb{R}^{21}$, and $\delta\hat{\boldsymbol{y}} \in \mathbb{R}^{7}$ are defined as,

$$\boldsymbol{u} = \left[\tilde{\boldsymbol{\omega}}^{b\,T},\ \tilde{\boldsymbol{f}}^{b\,T},\ \boldsymbol{\eta}_{g\delta b}^{T},\ \boldsymbol{\eta}_{f\delta b}^{T}\right]^{T} \tag{20e}$$

$$\delta\hat{\boldsymbol{x}} = \left[\delta\hat{\boldsymbol{e}}^{T},\ \delta\hat{\boldsymbol{v}}^{n\,T},\ \delta\hat{\boldsymbol{p}}^{n\,T},\ \hat{\boldsymbol{b}}_{g}^{T},\ \hat{\boldsymbol{b}}_{f}^{T},\ \delta\hat{\boldsymbol{b}}_{g}^{T},\ \delta\hat{\boldsymbol{b}}_{f}^{T}\right]^{T} \tag{20f}$$

$$\delta\hat{\boldsymbol{y}} = \left[\hat{\psi} - \hat{\psi}_{m},\ \delta\hat{\boldsymbol{y}}_{v}^{T},\ \delta\hat{\boldsymbol{y}}_{p}^{T}\right]^{T} \tag{20g}$$

$$\delta\hat{\boldsymbol{y}}_{v} = \left[\hat{\boldsymbol{v}}^{n} - \tilde{\boldsymbol{v}}_{GPS} - \left(\left[\hat{\boldsymbol{\omega}}_{ie}^{n}\times\right] + \left[\hat{\boldsymbol{\omega}}_{en}^{n}\times\right]\right)\hat{C}_{b}^{n}\,\boldsymbol{l}_{ba}^{b} + \hat{C}_{b}^{n}\left[\hat{\boldsymbol{\omega}}_{c}^{b}\times\right]\boldsymbol{l}_{ba}^{b}\right] \tag{20h}$$

$$\delta\hat{\boldsymbol{y}}_{p} = \hat{T}_{p}^{r}\left(\hat{\boldsymbol{p}}^{n} - \tilde{\boldsymbol{p}}_{GPS}^{n}\right) + \hat{C}_{b}^{n}\,\boldsymbol{l}_{ba}^{b} \tag{20i}$$

$$\hat{T}_{p}^{r} = \text{diag}\left(\left[(\hat{R}_{M} + \hat{h}),\,(\hat{R}_{N} + \hat{h})\cos(\hat{\gamma}),\,1\right]\right) \tag{20j}$$

where $\boldsymbol{l}_{ba}^{b}$ is the lever arm from the IMU to the GPS antenna, $\hat{T}_{p}^{r}$ is the curvilinear-to-Cartesian position change transformation matrix [6, Eq. 12.81, p. 391].

Being $I_{\{3\times3\}}$ an identity matrix and $\mathbf{0}_{\{3\times3\}}$ a null matrix, continuous and discrete state-space models matrices are defined as,

$$F_{(t)\{21\times21\}} = \begin{bmatrix} F_{ee} & F_{ev} & F_{ep} & -\hat{C}_{b}^{n} & \mathbf{0} & -\hat{C}_{b}^{n} & \mathbf{0} \\ F_{ve} & F_{vv} & F_{vp} & \mathbf{0} & \hat{C}_{b}^{n} & \mathbf{0} & \hat{C}_{b}^{n} \\ \mathbf{0} & F_{pv} & F_{pp} & \mathbf{0} & \mathbf{0} & \mathbf{0} & \mathbf{0} \\ \mathbf{0} & \mathbf{0} & \mathbf{0} & \mathbf{0} & \mathbf{0} & \mathbf{0} & \mathbf{0} \\ \mathbf{0} & \mathbf{0} & \mathbf{0} & \mathbf{0} & \mathbf{0} & \mathbf{0} & \mathbf{0} \\ \mathbf{0} & \mathbf{0} & \mathbf{0} & \mathbf{0} & \mathbf{0} & -\frac{1}{\boldsymbol{\tau}_{g}} & \mathbf{0} \\ \mathbf{0} & \mathbf{0} & \mathbf{0} & \mathbf{0} & \mathbf{0} & \mathbf{0} & -\frac{1}{\boldsymbol{\tau}_{f}} \end{bmatrix} \tag{20k}$$

$$G_{\{21\times12\}} = \begin{bmatrix} -\hat{C}_{b}^{n} & \mathbf{0} & \mathbf{0} & \mathbf{0} \\ \mathbf{0} & \hat{C}_{b}^{n} & \mathbf{0} & \mathbf{0} \\ \mathbf{0} & \mathbf{0} & \mathbf{0} & \mathbf{0} \\ \mathbf{0} & \mathbf{0} & \mathbf{0} & \mathbf{0} \\ \mathbf{0} & \mathbf{0} & \mathbf{0} & \mathbf{0} \\ \mathbf{0} & \mathbf{0} & I & \mathbf{0} \\ \mathbf{0} & \mathbf{0} & \mathbf{0} & I \end{bmatrix} \tag{20l}$$

$$H_{\{7\times21\}} = \begin{bmatrix} [0\,0\,1] & 0 & \cdots & \cdots & \cdots & \cdots & 0 \\ \mathbf{0} & I & \mathbf{0} & \mathbf{0} & \mathbf{0} & \mathbf{0} & \mathbf{0} \\ \mathbf{0} & \mathbf{0} & \hat{T}_{p}^{r} & \mathbf{0} & \mathbf{0} & \mathbf{0} & \mathbf{0} \end{bmatrix}. \tag{20m}$$

Submatrices F_{xx} are shown in [5, Eq. 12.28, p. 345].

Covariance matrix Q [6, Eq. 12.67, p. 387] is defined as,

$$Q_{\{12\times12\}} = \text{diag}\left(\left[\boldsymbol{n}_{g}^{2\,T},\,\boldsymbol{n}_{f}^{2\,T},\,\boldsymbol{n}_{g\delta b}^{2\,T},\,\boldsymbol{n}_{f\delta b}^{2\,T}\right]\right) \tag{21}$$

where $\boldsymbol{n}_{g}^{2}$, $\boldsymbol{n}_{f}^{2}$, $\boldsymbol{n}_{g\delta b}^{2}$, and $\boldsymbol{n}_{f\delta b}^{2}$ are the power spectral densities (PSD) of, respectively, the gyroscopes random noise, accelerometers random noise, gyroscopes dynamic bias, and accelerometers dynamic bias. $\boldsymbol{n}_{g\delta b}^{2}$ and $\boldsymbol{n}_{f\delta b}^{2}$ are obtained as [6, Eq. 12.68 and 12.69, p. 387],

$$\boldsymbol{n}_{g\delta b}^{2} = \boldsymbol{\sigma}_{g\delta b}^{2} \circ \boldsymbol{\tau}_{g} \tag{22a}$$

$$\boldsymbol{n}_{f\delta b}^{2} = \boldsymbol{\sigma}_{f\delta b}^{2} \circ \boldsymbol{\tau}_{f} \tag{22b}$$

where the symbol '$\circ$' means entrywise product, and $\boldsymbol{\tau}_{g}$ and $\boldsymbol{\tau}_{f}$ are correlation times of gyroscopes and accelerometers, respectively.

Covariance matrix R is defined as,

$$R_{\{7\times7\}} = \text{diag}\left(\left[\sigma_{\psi m}^{2},\,\boldsymbol{\sigma}_{v}^{2\,T},\,\sigma_{\gamma}^{2},\,\sigma_{\lambda}^{2},\,\sigma_{h}^{2}\right]\right) \tag{23}$$

where $\sigma_{\psi m}$ is the magnetic heading accuracy (Sec. III-A6) and $\boldsymbol{\sigma}_v$, σ_γ, σ_λ, and σ_h represent the GPS errors characteristics (Sec. II-D). The use of matrix $\hat{T}_p^r$ in Eq. 20i lets σ_γ and σ_λ be in units of meters. Then, terms of Eq. 23 are of the same order, which produces better numerical stability in calculating the Kalman gain, K.

Algorithm 1 presents a modified version of the EKF algorithm for one iteration. At each iteration, the state prediction equation reduces to $\delta\hat{\boldsymbol{x}}^- = \mathbf{0}$ [5, Eq. 13.9, p. 406], which is the optimal predicted error estimates. Hence, the original equation to update the actual state estimates $\delta\hat{\boldsymbol{x}} = \delta\hat{\boldsymbol{x}}^- + K(\delta\hat{\boldsymbol{y}} - \delta\hat{\boldsymbol{x}}^-)$ is simplified, as shown in line 5 of Alg. 1.

Algorithm 1 Simplified extended Kalman filter

1: Update $\delta t_{_G} = t_{_G} - t_{_{G(-)}}$, $\delta\hat{\boldsymbol{y}}$ (Eq. 20g), F (Eq. 20k), and G (Eq. 20l).
2: $\Phi \quad = I + F\,\delta t_{_G}$
3: $Q_k \;= G\;Q\;G^T\,\delta t_{_G}$
4: $K \quad = \left(P\;H^T\right)\left(R + H\;P\;H^T\right)^{-1}$
5: $\delta\hat{\boldsymbol{x}} \;= K\delta\hat{\boldsymbol{y}}$
6: $P_t \quad = (I - K\;H)\;\;P$
7: $P_{(+)} = \Phi\;P_t\;\Phi^T + Q_k$
8: $P_{(+)} = \frac{1}{2}\left(P_{(+)} + P_{(+)}^T\right)$

Since the master clock of our UMM is the GPS clock, the EKF evolves between GPS time steps, $t_{_G}$.

The covariance matrix $P_{\{21\times 21\}}$ must be set up initially before execution of Alg. 1. It is formed as a diagonal matrix whose individual elements are chosen according to the expected initial variances of $\delta\hat{\boldsymbol{x}}$ (Eq. 20f) as,

$$P_{(1)} = \text{diag}\left([\sigma_\phi^2,\, \sigma_\theta^2,\, \sigma_{\psi m}^2,\, \boldsymbol{\sigma}_v^{2\,T},\, \sigma_\gamma^2,\, \sigma_\lambda^2,\, \sigma_h^2,\, \boldsymbol{b}_g^2,\, \boldsymbol{b}_f^2,\, \boldsymbol{\sigma}_{g\delta b}^2,\, \boldsymbol{\sigma}_{g\delta f}^2]\right)\,. \tag{24}$$

Kalman filter may have serious numerical problems [11, Ch. 6, p. 225]. To avoid this situation, it is necessary but not sufficient that covariance matrix P be symmetric at each iteration. Line 8 of Alg. 1 ensures this condition [4, Sec. 5.9, p. 196].

IV. UMM ALGORITHM

A fundamental part of our UMM is the algorithm that exhibits the sequence in which equations shown in previous sections must be solve. This section shows the UMM algorithm and explains some aspects of our UMM.

Our UMM considers that discrete-time series $\tilde{\boldsymbol{\omega}}^b$, $\tilde{\boldsymbol{f}}^b$, and $\tilde{\boldsymbol{m}}^b$ are synchronized, i.e., they are all associated with the same vector time $t_{_S}$, which has a number of elements equal to $k_{_S}$. On the other hand, GPS discrete-time series $\tilde{\boldsymbol{p}}_{_{GPS}}^n$ and $\tilde{\boldsymbol{v}}_{_{GPS}}^n$ are associated with the vector time $t_{_G}$, which has a number of elements equal to $k_{_G}$. Since most low-cost GPS receivers deliver estimates at lower frequencies than an inertial measurement unit (IMU), it implies that $k_{_G} < k_{_S}$.

As said, the master clock of our UMM is the GPS clock. The EKF is only updated when new GPS data is available. Between GPS measurements, the SINS/MAG system keeps updating estimates of attitude, velocity, position, and magnetic heading angle.

Attitude is initialized with initial roll and pitch estimates and the magnetic heading angle, usually at rest. Position and velocity are initialized with corresponding GPS measurements.

Algorithm 2 details the operation of our UMM. All variables are in units of the International System of Units (SI).

State vector $\hat{\boldsymbol{x}}$ is defined as,

$$\hat{\boldsymbol{x}} = [\hat{\boldsymbol{e}}^T,\; \hat{\boldsymbol{v}}^{nT},\; \hat{\boldsymbol{p}}^{nT},\; \hat{\boldsymbol{b}}_{g(-)}^T,\; \hat{\boldsymbol{b}}_{f(-)}^T,\; \delta\hat{\boldsymbol{b}}_{g(-)}^T,\; \delta\hat{\boldsymbol{b}}_{f(-)}^T]^T\,. \tag{25}$$

Formulas for quaternions correction are [8, Eq. 7.34, A.172a, and A.173],

$$\hat{\boldsymbol{q}} = \hat{\boldsymbol{q}} + \frac{1}{2}\Xi(\hat{\boldsymbol{q}})\delta\hat{\boldsymbol{e}} \tag{26a}$$

$$\Xi(\hat{\boldsymbol{q}})_{\{4\times 3\}} = \begin{bmatrix} q_4\, I_{\{3\times 3\}} + [\boldsymbol{\varrho}\times] \\ -\boldsymbol{\varrho}^T \end{bmatrix} \tag{26b}$$

where $\boldsymbol{\varrho}$ comes from Eq. 12 and $\delta\hat{\boldsymbol{e}}$ is delivered by the EKF (Eq. 20f).

V. VALIDATION METHOD

The method to validate the proposed UMM takes a practical approach. We set up three integrated navigation systems using data sets that were collected on field, from three different MEMS IMU and a GPS. Then, we analyze if obtained performances are coherent with the quality of used sensors.

Algorithm 2 UMM algorithm.

Set $\boldsymbol{b}_g$, $\boldsymbol{b}_f$, $\boldsymbol{\sigma}_{g\delta b}$, $\boldsymbol{\sigma}_{f\delta b}$, $\boldsymbol{\tau}_g$, and $\boldsymbol{\tau}_f$
Set $\boldsymbol{n}_g$, $\boldsymbol{n}_f$, $\boldsymbol{n}_{g\delta b}$, and $\boldsymbol{n}_{f\delta b}$
Set σ_γ, σ_λ, σ_h, and $\boldsymbol{\sigma}_v$
Set σ_ϕ, σ_θ, $\sigma_{\psi m}$, and D ([12])
Load $\tilde{\boldsymbol{\omega}}^b$ (Eq. 1), $\tilde{\boldsymbol{f}}^b$ (Eq. 3), and $\tilde{\boldsymbol{m}}^b$ (Eq. 5)
Load $\tilde{\boldsymbol{p}}^n_{_{GPS}}$ (Eq. 6), and $\tilde{\boldsymbol{v}}^n_{_{GPS}}$ (Eq. 8)
Calculate $\hat{\psi}_{m(1)}$ (Eq. 19)
Set $\hat{\boldsymbol{e}}_{(1)} = [\hat{\phi}_{(1)}, \hat{\theta}_{(1)}, \hat{\psi}_{m(1)}]$
Set $\hat{\boldsymbol{p}}^n_{(1)} = \tilde{\boldsymbol{p}}^n_{_{GPS(1)}}$ and $\hat{\boldsymbol{v}}^n_{(1)} = \tilde{\boldsymbol{v}}^n_{_{GPS(1)}}$
Calculate $\hat{\boldsymbol{q}}_{(1)}$ with $\hat{\boldsymbol{e}}_{(1)}$ (see [5, Eq. 3.65, p.46])
Calculate $\hat{C}^n_{b(1)}$ with $\hat{\boldsymbol{q}}_{(1)}$ (14)
Set $\hat{\boldsymbol{b}}_g = \mathbf{0}$, $\hat{\boldsymbol{b}}_f = \mathbf{0}$, $\delta\hat{\boldsymbol{b}}_g = \mathbf{0}$, and $\delta\hat{\boldsymbol{b}}_f = \mathbf{0}$
Set Q (Eq. 21), R (Eq. 23), and $P_{(1)}$ (Eq. 24)
Set $i = 2$
for $k = 2$ to $k_{_G}$ **do**
    while $t_{_{S(i)}} =< t_{_{G(k)}}$ **do**
        Update $\hat{\boldsymbol{\omega}}^n_{ie}$ and $\hat{\boldsymbol{\omega}}^n_{en}$ (Eq. 9 and 10).
        Update $\hat{\boldsymbol{q}}$ (Eq. 13)
        Update $\hat{C}^n_b$ (Eq. 14)
        Update $\hat{\boldsymbol{e}}$ (Eq. 15)
        Update $\hat{\boldsymbol{g}}^n$ (Eq. 16)
        Update $\hat{\boldsymbol{v}}^n$ (Eq. 17)
        Update $\hat{\boldsymbol{p}}^n$ (Eq. 18)
        Update $\hat{\psi}_m$ (Eq. 19)
        $i = i + 1$
    end while
    Update $\delta\hat{\boldsymbol{x}}$ (Alg. 1)
    Correct $\hat{\boldsymbol{x}}$: $\hat{\boldsymbol{x}} = \hat{\boldsymbol{x}} - \delta\hat{\boldsymbol{x}}$
    Correct $\hat{\boldsymbol{q}}$ (Eq. 26)
    Correct $\hat{C}^n_b$ (Eq. 14)
end for

A. Experiment setup

In [13], several grade IMU and a Novatel OEM4 dual-frequency GPS receiver were mounted on a vehicle. Measurements from these sensors were logged for several open-sky trajectories. In addition, a DGPS system was implemented using a Topcon Legacy GPS base station. Among all the available trajectories, we choose the trajectory labeled as 8, which contains high and low dynamics. We only consider the first 9 minutes, throughout which the availability of GPS signal is 100%. Lever arm vectors were provided.

We select three MEMS IMU, namely, Xbow IMU400CD (XBOW1), Xsens MTi (XSENS1), and Gladiator Landmark 10 (GLAD), and implement three integrated systems, XBOW1/GPS, XSENS1/GPS, and GLAD/GPS. A reference data set is obtained fusing navigation-grade Honeywell IMU H764G-1 and DGPS measurements.

Since IMU data sets lack of magnetometers information, vector $\delta\hat{\boldsymbol{y}}$ (Eq. 20g) must be reduced to $\delta\hat{\boldsymbol{y}} = \left[\delta\hat{\boldsymbol{y}}_v^T,\ \delta\hat{\boldsymbol{y}}_p^T\right]^T$. As a consequence, order of matrices H (Eq. 20m) and R (Eq. 23) also decreases accordingly.

The same three MEMS IMU units used in [13] were profiled in [14], in which IMU units error characteristics were determined by using the Allan variance and PSD techniques. Then, MEMS IMU noises terms are taken from [14, Table 4.4, p. 73], except static bias that is taken from [14, Table 4.3, p. 65], which are shown in Table III for completeness. It can be seen from Table III that XBOW1 and XSENS1 are of similar quality, and, on the other hand, GLAD presents a lower quality. GSP position error is 1.5m CEP, and $\boldsymbol{\sigma}_v = 0.03$, as stated in the GPS datasheet [15].

B. Result analysis

The UMM is programmed in MATLAB. Table IV displays the RMS errors with respect to the reference data set, for the three proposed integrated systems and GPS-only solution.

Analyzing values of columns from Table IV, it can be seen that XBOW1/GPS and XSENS1/GPS performances are similar, since these IMU have also similar error characteristics. On the other hand, GLAD/GPS system shows a worse performance,

Table III
IMU ERROR CHARACTERISTICS (TAKEN FROM [14, TABLE 4.4, P. 73]).

			XBOW1	XSENS1	GLAD
ARW (n_g)	$\frac{\text{deg/s}}{\sqrt{\text{Hz}}}$	X	3.996E-2	8.230E-2	1.418E-1
		Y	3.141E-2	7.802E-2	1.364E-1
		Z	3.581E-2	8.948E-2	1.338E-1
VRW (n_f)	$\frac{\text{m/s}^2}{\sqrt{\text{Hz}}}$	X	1.353E-3	1.493E-3	4.094E-2
		Y	1.353E-3	1.589E-3	4.104E-2
		Z	9.850E-4	1.793E-3	4.231E-2
b_g	deg/s	X	0.441	2.425	0.061
		Y	0.040	0.574	0.322
		Z	0.114	0.104	0.895
b_f	m/s^2	X	-0.151	0.307	0.173
		Y	0.007	-0.280	0.173
		Z	9.829	9.869	9.822
δb_g	deg/s	X	3.427E-3	1.142E-2	1.154E-2
		Y	2.028E-3	1.230E-2	1.200E-2
		Z	2.153E-3	1.526E-2	1.154E-2
δb_f	m/s^2	X	1.787E-4	4.274E-4	3.232E-3
		Y	1.843E-4	3.396E-4	3.171E-3
		Z	2.149E-4	4.769E-4	3.610E-3
τ_g	s	X	250.7	274.4	458.9
		Y	432.2	463.9	289.7
		Z	395.2	132.2	370.9
τ_f	s	X	196.9	33.4	260.2
		Y	332.8	124.3	382.8
		Z	79.6	39.2	351.3

Table IV
RMS ERRORS FOR THE THREE INTEGRATED SYSTEMS.

		XBOW1/GPS	XSENS1/GPS	GLAD/GPS	GPS only
ϕ	deg	0.126	0.305	0.902	–
θ	deg	0.130	0.274	1.295	–
ψ	deg	3.084	2.529	4.401	–
v_N	m/s	0.066	0.068	0.209	0.195
v_E	m/s	0.048	0.040	0.220	0.154
v_D	m/s	0.009	0.011	0.401	0.042
γ	m	0.185	0.192	0.279	0.663
λ	m	0.180	0.178	0.289	0.517
h	m	0.249	0.235	0.587	0.195

which is coherent with GLAD quality. Moreover, it can be seen that the three integrated systems present smaller horizontal-position RSM errors than the GPS-only solution, and these horizontal errors are proportional to IMU qualities. All these are expected scenarios.

VI. CONCLUSIONS

In this work, a unified mathematical model for low-cost integrated navigation systems is presented. This paper exposes the complete mathematical model of a loosely-couple SINS/MAG/GPS system, as well as the mathematical models of inertial sensors, magnetometers and a GPS receiver. Our UMM is based on classical navigation equations and intended to be used as a benchmark for low-cost integrated navigation systems, against which novel solution to the navigation problem can be objectively contrasted.

Validation of our UMM is achieved through processing real-world data sets from three MEMS IMU and a GPS receiver. It is shown that performances of the three processed integrated navigation system are coherent with corresponding MEMS IMU error characteristics.

In conclusion, the proposed unified mathematical model is a suitable integrated navigation model, and a useful benchmark to evaluate new solutions related to low-cost integrated navigation systems.

ACKNOWLEDGMENTS

The authors would like to thank to Dr. C. Toth, Dr. A. Kealy, and Msc. A.H. Rabiain for generously share IMU and GPS data sets, and, in particular, for Msc. Rabiain's unselfish support. They also would like to thank to Dr. C.A. Catania for his continuous help.

FUNDING

This work was supported by the National Agency for Scientific and Technological Promotion, Argentina; and the National Technological University, Argentina.

REFERENCES

[1] R. van der Merwe and E. A. Wan, "Sigma-point Kalman filters for integrated navigation," in *Proceedings of the 60th Annual Meeting of The Institute of Navigation*, pp. 641–654, June 2004.
[2] S. Godha and M. E. Cannon, "Integration of DGPS with a low cost MEMS - Based inertial measurement unit (IMU) for land vehicle navigation application," in *Proceedings of the 18th International Technical Meeting of the Satellite Division of The Institute of Navigation (ION GNSS 2005)*, (Long Beach, CA), pp. 333–345, September 2005.
[3] A. K. Brown and Y. Lu, "Performance test results on an integrated gps/mems inertial navigation package.," in *Proceedings of ION GNSS 2004*, (Long Beach, CA), September 2004.
[4] J. Farrell, *Aided Navigation: GPS With High Rate Sensors*. USA: McGraw-Hill Professional, March 2008.
[5] D. H. Titterton and J. L. Weston, *Strapdown Inertial Navigation Technology*. USA: Institution of Engineering and Technology, 2nd ed., 2004.
[6] P. D. Groves, *Principles of GNSS, Inertial, and Multisensor Integrated Navigation Systems*. USA: Artech House, 2008.
[7] G. Cai, B. M. Chen, and T. H. Lee, *Unmanned Rotorcraft Systems*. UK: Springer London, 2011.
[8] J. L. Crassidis and J. L. Junkins, *Optimal Estimation of Dynamic Systems*. USA: Chapman and Hall/CRC, 2nd ed., 2011.
[9] M. J. Caruso, "Applications of magnetic sensors for low cost compass systems," in *Position Location and Navigation Symposium, IEEE 2000*, pp. 177–184, 2000.
[10] R. G. Brown and P. Y. C. Hwang, *Introduction to Random Signals and Applied Kalman Filtering*. USA: John Wiley & Sons, Inc., 3rd ed., 1997.
[11] M. S. Grewal and A. P. Andrews, *Kalman Filtering: Theory and Practice Using MATLAB*. USA: John Wiley & Sons, Inc., 3rd ed., 2008.
[12] National Geophysical Data Center, July 2013.
[13] C. Toth, D. Brzezinska, N. Politi, and A. Kealy, "Reference data set for performance evaluation of MEMS-based integrated navigation solutions," in *FIG Working Week 2011*, (Marrakech, Morocco), pp. 1–10, May 2011.
[14] A. H. Rabiain, "Performance evaluation of MEMS based INS/GPS integration," Master's thesis, Department of Geomatics, The University of Melbourne, December 2010.
[15] Novatel Inc., *OEM4 Family, User Manual (OM-20000046 Rev 19)*, December 2005.